Cadmium promotes glycolysis upregulation and glutamine dependency in human neuronal cells

Federica Bovio[a], Pasquale Melchioretto[b], Matilde Forcella[a], Paola Fusi[a,c], Chiara Urani[b,c]

[a]*Department of Biotechnology and Biosciences, University of Milano-Bicocca, Piazza della Scienza, 2, 20126 Milan, Italy*

[b]*Department of Earth and Environmental Sciences, University of Milan Bicocca, Piazza della Scienza 1 20126 Milan, Italy*

[c]*Integrated Models for Prevention and Protection in Environmental and Occupational Health, (MISTRAL), Interuniversity Research Center*

Corresponding author: Matilde Forcella and Paola Fusi

E-mail addresses: f.bovio@campus.unimib.it (F. Bovio), pasquale.melchioretto@unimib.it (P. Melchioretto), matilde.forcella@unimib.it (M. Forcella), paola.fusi@unimib.it (P. Fusi), chiara.urani@unimib.it (C. Urani)

Abstract

Cadmium is a widespread pollutant, which easily accumulates inside the human body with an estimated half-life of 25-30 years. Many data strongly suggest that it may play a role in neurodegenerative diseases pathogenesis. In this paper we investigated cadmium effect on human SH-SY5Y neuroblastoma cells metabolism. Results showed that, although SH-SY5Y cells already showed hyperactivated glycolysis, cadmium further increased basal glycolytic rate. Both glycolytic capacity and reserve were also increased, following cadmium administration, endowing the cells with a higher compensatory glycolysis when oxidative phosphorylation was inhibited. Cadmium administration also led to an increase in glycolytic ATP production rate, paralleled by a decrease in ATP production by oxidative phosphorylation, due to an impairment of mitochondrial respiration. Moreover, following cadmium administration, mitochondria increased their dependency on glutamine, while decreasing lipids oxidation. On the whole, our data show that cadmium exacerbates the Warburg effect and promotes the use of glutamine as a substrate for lipid biosynthesis. Although increased glutamine consumption leads to an increase in glutathione level, this cannot efficiently counteract cadmium-induced oxidative stress, leading to membrane lipid peroxidation. Oxidative stress represents a serious threat for neuronal cells and our data confirm glutathione as a key defense mechanism.

Keywords

Energy metabolism, cadmium, SH-SY5Y neuronal cells, glutamine, glutathione, oxidative stress

1. Introduction

The rare heavy metal cadmium (Cd), found in air, water and sediment with a concentration of 0.15 mg/kg in the Earth crust and of 1.1×10^{-4} mg/L in the sea, is widely used in both industry and agriculture, leading to its widespread diffusion into the environment (Zhang and Reynolds, 2019). The absence of a biodegradation system united to its toxicity and accumulation in organisms, with an estimated half-life of 25-30 years in humans, led the scientific community to classify this metal as part of the group of main environmental and occupational chemical pollutants in industrialized countries (Mezynska and Brzóska, 2018).

Since cadmium uptake can occur through inhalation of polluted air, cigarette smoking or ingestion of contaminated food and water, the main routes of its entry into human body are the respiratory and the gastrointestinal tract, accounting respectively for the 10-40% and 5-8% of the load, with the skin playing a minor role (Nordberg, 2009; Sabolić et al., 2010; Sarkar et al., 2013). Once inside, the majority of cadmium is stored in the liver and kidneys, which help spreading its toxicity; however, this metal can affect also lungs, testis, cardiovascular and nervous systems.

Under normal conditions, cadmium can barely cross the blood brain barrier (BBB), reaching the central nervous system (CNS); however, if present in the blood stream, it can enter the cells through channels, transporters and receptors placed on the luminal surface of the BBB endothelial cells (Thévenod et al., 2019). In case of acute cadmium exposure, the BBB protects the majority of the CNS; while in chronic and prolonged exposures, cadmium is responsible for weakening the cellular antioxidant defences and increasing reactive oxygen species (ROS) formation, with the consequent activation of matrix metalloproteinases that disrupt BBB tight junctions and enhance its permeability (Branca et al., 2020; Yang et al., 2007). Another route of cadmium uptake in the CNS is represented by the nasal mucosa or olfactory pathways, with the metal, transported along primary olfactory neurons, reaching the terminations in the olfactory bulbs and bypassing the intact BBB (Tjälve and Henriksson, 1999).

Once in the brain, this metal accumulates in the choroid plexus in concentrations much greater than those found in the cerebrospinal fluid (Wang and Du, 2013). Having an abundant pool of metal binding ligands responsible for metal ions binding, such as metallothioneins, and a highly active antioxidant defence system, like the antioxidant enzymes superoxide dismutase and catalase, makes the choroid plexus the first line of defence against cadmium toxicity in the CNS (Zheng et al., 1991). However, none of the cellular defence mechanisms is perfectly efficient and the consequences of cadmium exposure act on several molecular pathways.

Even though the exact mechanisms through which cadmium exerts its neurotoxicity are still unresolved, one of its main targets is the mitochondrion, which can suffer several damages triggered by this metal. Cadmium can act on complex II (succinate dehydrogenase) and complex III (cytochrome bc1 complex) inducing the inhibition of the electron transport chain (ETC) and ATP production, which results in the formation of ROS favoured by the high $NADH/NAD^+$ ratio present in the matrix (Brand, 2016). In particular the principal site of ROS production seems to reside in complex III, and ROS accumulation disrupts the mitochondrial membrane potential, activating a sequence of events (Genchi et al., 2020). This altered membrane potential leads to an

increase in mitochondrial membrane permeability, followed by the release of cytochrome *c* through the opening of transition pore with consequent activation of the caspase pathway (Oh and Lim, 2006). Additionally, cadmium has been reported to inhibit ATPase, to enhance the level of lipid peroxidation and to alter the cellular redox status by reacting with exogenous and endogenous antioxidants, such as reduced glutathione (Cannino et al., 2009; Cuypers et al., 2010).

Al-Ghafari and colleagues showed a loss in the ETC of cadmium-exposed osteoblasts together with a reduced ATP production and oxygen consumption, that correlate with an increase in lactate production, suggesting a shift to anaerobic metabolism (Al-Ghafari et al., 2019). Moreover, a metabolomic study on neuronal PC-12 cells confirmed the increase in lactic acid content, which could be a reflection of enhanced glycolysis due to inadequate energy supply through oxidative phosphorylation (Zong et al., 2018). However this increase in glycolytic activity happens in the initial phase of exposure, while a chronic exposure inhibits glycolysis due to negative effects on hexokinase, phosphofructokinase and pyruvate kinase caused by cadmium binding to the sulfhydryl (-SH) groups of the mentioned enzymes (Li et al., 2016; Sabir et al., 2019). Subsequently, cell energy production is likely obtained by proteins oxidation, since cadmium increases the activity of several enzymes involved in amino acids catabolism, such as amino acid oxidase, glutamate dehydrogenase and xanthine oxidase (Sabir et al., 2019).

To better understand the role of cadmium in the mechanisms of neurodegeneration, in the present work we have evaluated the mitochondrial status and the energy metabolism of SH-SY5Y neuronal cells treated with 10 µM and 20 µM $CdCl_2$ for 24 hours, by measuring the oxygen consumption rate and the extracellular acidification rate through Seahorse technology. In addition, due to the recognized role of lipid peroxidation as an important factor in the development of neurodegenerative disorders (Peña-Bautista et al., 2019), we have analysed the oxidative status in SH-SY5Y cells under the same cadmium treatment conditions. Our results show a decrease of mitochondria functionality, together with an enhanced glycolysis, following cadmium treatment, suggesting a shift to anaerobiosis due to mitochondrial damage; this is confirmed by a greater glycolytic ATP production in cadmium treated cells. Moreover, regarding the evaluation of mitochondrial fuel oxidation, cadmium treatment led to an increase in glutamine dependency, suggesting the use of proteins for energy production.

2. Materials and methods

2.1. Mammalian cell culture

SH-SY5Y (ATCC® HTB-2266™) human neuroblastoma cell line was grown in F12:EMEM (1:1) medium supplemented with heat-inactivated 10% FBS, 2 mM L-glutamine, 100 U/mL penicillin, 100 µg/mL streptomycin and maintained at 37 °C in a humidified 5% CO_2 incubator. ATCC validated cell line by short tandem repeat profiles that are generated by simultaneous amplification of multiple short tandem repeat loci and amelogenin (for gender identification). All the reagents for cell culture were supplied by EuroClone (Pero, Milan, Italy).

2.2. Cell viability assay

Cell viability was investigated using *in vitro* toxicology assay kit MTT-based, according to manufacturer's protocols (Merck KGaA, Darmstadt, Germany).

In order to evaluate cadmium toxicity, cells were seeded in 96-well micro-titer plates at a density of 1×10^4 cells/well and after 24 hours were treated with different $CdCl_2$ concentrations (0-200 μM). After 24 hours at 37 °C, the medium was replaced with a complete medium without phenol red and 10 μL of a 5 mg/mL MTT (3-(4,5-dimethylthiazol-2)-2,5-diphenyltetrazolium bromide) solution was added to each well. After a further incubation for 4 hours, upon formed formazan crystals solubilization with 10% Triton-X-100 in acidic isopropanol (0.1 N HCl), absorbance was measured at 570 nm using a micro plate reader. Viabilities were expressed as a percentage of the untreated controls. Each experiment was performed in three replicate wells for each metal concentration and results are presented as the mean of at least three independent experiments.

2.3. Oxygen consumption rate and extra-cellular acidification rate measurements

Oxygen consumption rate (OCR) and extra-cellular acidification rate (ECAR) were investigated using Agilent Seahorse XFe96 Analyzer on SH-SY5Y cell line treated with cadmium.

The cells were seeded in Agilent Seahorse 96-well XF cell culture microplates at a density of 4×10^4 cells per well in 180 μL of growth medium and were allowed to adhere for 24 h in a 37 °C humidified incubator with 5% CO_2. Subsequently the seeded cells were treated with $CdCl_2$ 10 μM or 20 μM for 24 hours. In addition, before running the assay, the Seahorse XF Sensor Cartridge was hydrated and calibrated with 200 μL of Seahorse XF Calibrant Solution in a non-CO_2 37 °C incubator in order to remove CO_2 from the media that would otherwise interfere with measurements that are pH sensitive.

After the 24 hours of cadmium treatment, for Agilent Seahorse XF Cell Energy Phenotype Test Kit, Agilent Seahorse XF ATP Rate Assay Kit, Agilent Seahorse XF Cell Mito Stress Test Kit and Agilent Seahorse XF Mito Fuel Flex Test Kit the growth medium was replaced with 180 μL/well of Seahorse XF Base Medium containing 1 mM pyruvate, 2 mM L-glutamine and 10 mM glucose; while for Agilent Seahorse XF Glycolysis Stress Test Kit the medium substitution was made with XF Base Medium containing 2 mM L-glutamine and with XF Base Medium containing 1 mM pyruvate, 2 mM L-glutamine, 10 mM glucose and 5 mM Hepes for Agilent Seahorse XF Glycolytic Rate Assay Kit. Subsequently the plate was incubated into a 37 °C non-CO_2 incubator for 1 hour, before starting the experimental procedure, and the compounds were loaded into injector ports of sensor cartridge.

For Agilent Seahorse XF Cell Energy Phenotype Test Kit a pre-warmed combined mixture of oligomycin and FCCP (carbonyl cyanide-4-(trifluoromethoxy)phenylhydrazone) was loaded into injector port A to reach working concentration of 1 μM and 2 μM respectively. OCR and ECAR were detected under basal conditions followed by the addition of the compounds to measure baseline phenotype, stressed phenotype and metabolic potential.

The OCR and ECAR detected during Agilent Seahorse XF Glycolysis Stress Test Kit allowed to measure the glycolytic function in cells (glycolysis, glycolytic capacity, glycolytic reserve and non-glycolytic acidification)

through the sequential additions of pre-warmed glucose, oligomycin and 2-deoxy-D-glucose (2-DG) into injector ports A, B and C to reach final concentration of 10 mM, 1 μM and 50 mM, respectively. Regarding Agilent Seahorse XF Glycolytic Rate Assay Kit, pre-warmed combination of rotenone and antimycin A at working concentration of 0.5 μM and 2-DG at 50 mM were loaded into injector ports A and B respectively. OCR and ECAR were detected under basal conditions followed by the sequential addition of the compounds in order to measure basal glycolysis, basal proton efflux rate, compensatory glycolysis and post 2-DG acidification.

Agilent Seahorse XF ATP Rate Assay Kit measures the total amount of ATP produced in living cells, distinguishing between the fractions of ATP derived from mitochondrial oxidative phosphorylation and glycolysis, through the detection of OCR and ECAR under basal conditions followed by the sequential addition of pre-warmed working concentration of 1.5 μM oligomycin in injector port A and of 1 μM rotenone and antimycin A into injector port B.

For Agilent Seahorse XF Cell Mito Stress Test Kit pre-warmed oligomycin, FCCP, rotenone and antimycin A were loaded into injector ports A, B and C of sensor cartridge at a final working concentration of 1 μM, 2 μM and 0.5 μM, respectively. OCR and ECAR were detected under basal conditions followed by the sequential addition of the compounds and non-mitochondrial respiration, maximal respiration, proton leak, ATP respiration, respiratory capacity and coupling efficiency can be evaluated. Using the Agilent Seahorse XF Mito Fuel Flex Test Kit the mitochondrial fuel usage in living cells has been determined and, through OCR measuring, the dependency, capacity and flexibility of cells to oxidize glucose, glutamine and long-chain fatty acids can be calculated. Pre-warmed working concentration of 3 μM BPTES, 2 μM UK5099 or 4 μM etomoxir were loaded into injector port A and compounds mixture of 2 μM UK5099 and 4 μM etomoxir, 3 μM BPTES and 4 μM etomoxir or 3 μM BPTES and 2 μM UK5099 into injector port B in order to determine glutamine, glucose and long-chain fatty acid dependency, respectively. On the contrary fuels capacity is measured by the addition into injector port A of 2 μM UK5099 and 4 μM etomoxir, 3 μM BPTES and 4 μM etomoxir or 3 μM BPTES and 2 μM UK5099 working concentration, followed by injection in port B of 3 μM BPTES, 2 μM UK5099 or 4 μM etomoxir working concentration for glutamine, glucose and long-chain fatty acid, respectively.

All the kits and reagents were purchased by Agilent Technologies (Santa Clara, CA, USA).

2.4. Lipid peroxidation assay

The extent of lipid peroxidation was determined by the levels of malondialdehyde (MDA) measured using the thiobarbituric acid reactive substances assay (Buege and Aust, 1978). SH-SY5Y cells were seeded at 1×10^6 cells/100 mm dish and, on the following day, were treated with either 10 μM or 20 μM $CdCl_2$. Twenty-four hours after the treatment, the cells were harvested by trypsinization, washed with PBS (10 mM K_2HPO_4, 150 mM NaCl, pH 7.2) and the resulting pellet was resuspended in 500 μL PBS. Cell lysis was obtained through sonication (15 sec at 10% amplitude 3 times) and protein content was determined by Bradford assay, using BSA for the calibration curve (Bradford, 1976). Subsequently 1 mL of a 15% TCA (trichloroacetic acid),

0.375% TBA (2-thiobarbituric acid) and 0.25 M HCl solution was added to the lysates, followed by a 15 minutes incubation at 95 °C. Subsequently, samples were centrifuged at 10,000 × g for 10 min, supernatants were collected and the absorbance at 530 nm was measured. Additionally, a background sample made by only PBS was treated in the same way. Lipid peroxidation level was expressed as nmol of MDA/mg protein using a molar extinction coefficient of 1.56×10^5 M^{-1} cm^{-1}. Results were reported as a percentage compared to untreated control and results are presented as the mean of at least three independent experiments.
All the chemicals were supplied by Merck KGaA, Darmstadt, Germany.

2.5. Glutathione detection

For the measurement of total glutathione (GSH tot), oxidized glutathione (GSSG) and reduced glutathione (GSH) content in cells treated with $CdCl_2$ for 24 hours, SH-SY5Y cells were seeded in 96-well micro-titer plates at a density of 2×10^4 cells/well. The day after seeding, the cells were exposed to either 10 μM or 20 μM $CdCl_2$ for 24 hours, with cells not treated with $CdCl_2$ representing the control.
At the end of the treatment, the cells were lysed in 100 μL/well of 1% SSA (Sulfosalicylic acid) and scraped to ensure complete lysis. The assays of total glutathione and GSSG were performed in a reaction mix containing 100 μM DTNB (5,5′-dithiobis(2-nitrobenzoic acid)), 200 μM NADPH and 0.46 U/mL glutathione reductase added to the GSH-buffer (100 mM Na_2HPO_4, 100 mM NaH_2PO_4, 1 mM EDTA, pH 7.5).
To measure total glutathione, 50 μL of each cell lysate were transferred into a new 96-well plate and 50 μL of MilliQ water were added. Then, 100 μL of reaction mixture were added to each well and absorbance at 405 nm was measured immediately after, as well as after 20 and 30 minutes using a micro plate reader. Additionally, a calibration curve was prepared (0-10 μM GSH) and treated like the samples.
For GSSG evaluation the 50 μL/well left were treated with 1 μL of 2-vinylpyridine solution (27 μL 2-vinylpyridine in 98 μL ethanol) for 1 hour at RT in order to block the SH-groups. Then 50 μL of MilliQ water and 100 μL of reaction mixture were added to each well and absorbance at 405 nm was measured immediately after, as well as after 20 and 30 minutes using a micro plate reader. Additionally, a calibration curve was prepared (0-10 μM GSSG) and treated like the samples.
The values of absorbance were compared to standard curves and converted into molarity of total glutathione and GSSG: GSH (GSH tot − GSSG) was calculated. Total glutathione was expressed as a percentage of the control; while GSSG and GSH were expressed as a percentage of total glutathione for each condition. Each experiment was performed in three replicate wells for each metal concentration and results are presented as the mean of at least three independent experiments.
All the chemicals were supplied by Merck KGaA, Darmstadt, Germany.

2.6. Glutathione S-transferase and glutathione reductase enzyme activity assays

In order to evaluate the effect of cadmium on glutathione S-transferase (GST) and glutathione reductase (GR) activities, SH-SY5Y cells were seeded at 2×10^6 cells/100 mm dish and, 24 hours later, exposed to either 10 μM or 20 μM $CdCl_2$ for 24 hours. Cells not treated with $CdCl_2$ represented the control. Subsequently, control

and cadmium treated cells were rinsed with ice-cold PBS (10 mM K_2HPO_4, 150 mM NaCl, pH 7.2) and lysed in 50 mM Tris/HCl, pH 7.4, 150 mM NaCl, 5 mM EDTA, 10% glycerol, 1% NP40 buffer, containing protease inhibitors and 1 mM PMSF. After lysis on ice, homogenates were obtained by passing the cells 5 times through a blunt 20-gauge needle fitted to a syringe and then centrifuging at 15,000 × g at 4 °C for 30 min. The resulting supernatant was used to measure GST activity according to Habig et al. (Habig et al., 1974) and GR activity according to Wang (Wang et al., 2001). Enzyme activities were expressed in international units and referred to protein concentration, quantified by Bradford assay, using BSA for the calibration curve (Bradford, 1976). All assays were performed in triplicate at 30 °C.

All chemicals were purchased by Merck KGaA, Darmstadt, Germany.

2.7. Statistical analysis

All the experiments were carried out in triplicate. The samples were compared to their reference controls and the data were tested by Dunnett multiple comparison procedure. Results were considered statistically significant at $p < 0.05$.

3. Results

3.1. Exposure to $CdCl_2$ affects neuronal cells viability

In order to determine $CdCl_2$ doses to be used in the analysis of oxidative stress and in Seahorse experiments, the effect of this metal was first evaluated on SH-SY5Y cells viability.

As reported in Figure 1, neuronal cells treated with $CdCl_2$ for 24 hours showed a dose-dependent reduction in their viability: while doses lower than 50 µM mildly affected the cell viability, with a 67% residual viability at 20 µM $CdCl_2$, higher concentrations strongly reduced viability, with only 13% residual viability at 200 µM; therefore, 10 µM and 20 µM $CdCl_2$ concentrations were used for our further experiments.

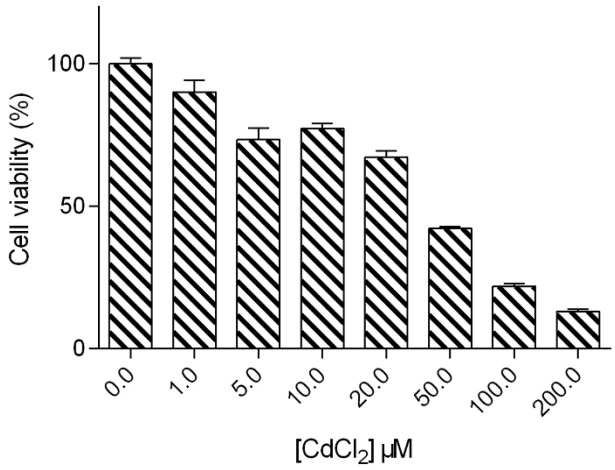

Fig. 1. SH-SY5Y viability in the presence of cadmium. Cell survival was determined by MTT assay, after a 24-hour incubation in the presence of different $CdCl_2$ concentrations (0–200 µM). Data are shown as means ± standard error (SEM).

3.2. Evaluation of SH-SY5Y energy phenotype shows that $CdCl_2$ treated cells increase basal glycolysis

In order to investigate if cadmium could cause a different response in cells when stressor compounds are administered, the energy metabolism of SH-SY5Y cells treated for 24 hours with either 10 µM or 20 µM $CdCl_2$ was analysed using the Agilent Seahorse XF Cell Energy Phenotype Test Kit.

Under basal conditions, the OCR level, measuring mitochondrial respiration rate in living cells, showed no difference among the samples (Fig. 2A and C); while the ECAR rate, which represents a measure of glycolysis, was found higher in cadmium treated cells (Fig. 2B and D). A simultaneous injection of oligomycin, an ATP synthase inhibitor, and FCCP, an uncoupling agent, determined an increase in both OCR and ECAR; however, while OCR level increased to the same extent in all the conditions studied (Fig. 2A and C), ECAR increase was higher for cadmium-treated cells than for control cells (Fig. 2B and D).

The percentage increase of stressed parameters over baseline ones is the metabolic potential, which is defined as the cells' ability to meet an energy demand via respiration and glycolysis. SH-SY5Y cells treated with cadmium showed the same metabolic potential of control cells for OCR, while showing a decreased metabolic potential for ECAR. In fact, as seen in Figure 2E, the latter showed a dose-dependent reduction following 24 hours Cd treatment, although statistically significant only at 20 µM $CdCl_2$.

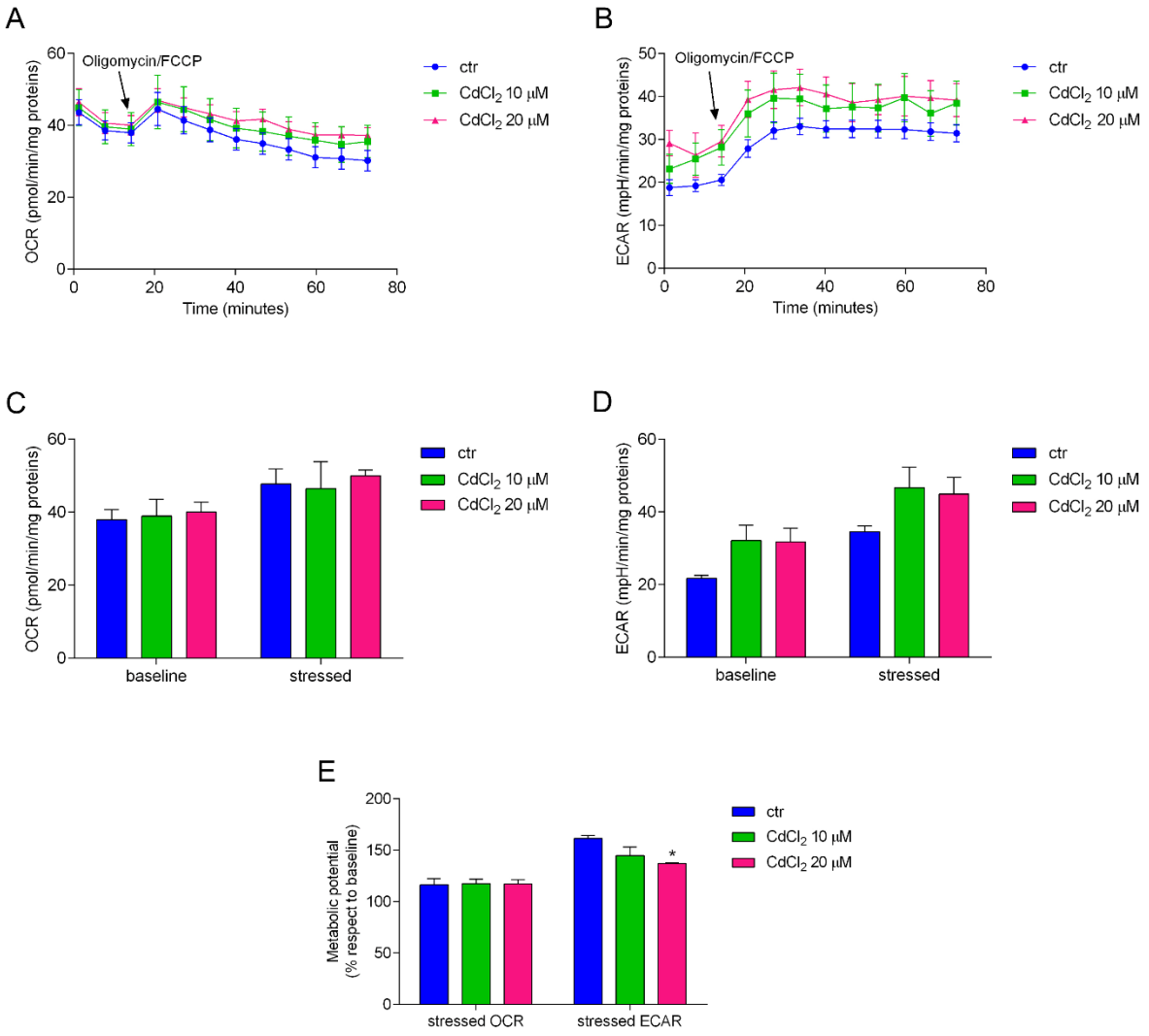

Fig. 2. Cell energy phenotype after 24-hour exposure to either 10 µM or 20 µM $CdCl_2$. OCR (A) and ECAR (B) traces, expressed as pmol O_2/min/mg proteins and mpH/min/mg proteins respectively, in control and $CdCl_2$-treated cells. The arrows indicate the time of simultaneous addition of oligomycin/FCCP. The OCR and ECAR profiles are representative of three independent experiments. Analysis of baseline and stressed level of mitochondrial respiration (C) and glycolysis (D) and metabolic potential (E). Bars indicate the mean ± SEM obtained in three independent experiments.

Statistically significant: * $p < 0.05$

3.3. $CdCl_2$ administration increases both glycolytic capacity and glycolytic reserve

The results obtained in the cell energy phenotype analysis led us to hypothesize an increased glycolysis level in cadmium-treated cells. In order to investigate the glycolytic functions, the glycolytic rate and the compensatory glycolysis Agilent Seahorse XF Glycolysis Stress Test Kit and Agilent Seahorse XF Glycolytic Rate Assay Kit were used.

The ECAR profile, reported in Figure 3A, determined after treatment with cadmium, showed a dose-dependent increase in protons extrusion both at the basal level and after the injection of a saturating concentration of

glucose; the administration of oligomycin and hexokinase inhibitor 2-deoxyglucose (2-DG) permitted, through modulation of ECAR, the analysis of glycolytic parameters. Extracellular acidification was found higher after cadmium administration. In particular, treatment with 20 µM $CdCl_2$ caused a significant increase in non-glycolytic acidification, as well as in glycolysis and glycolytic capacity; while following the 10 µM dose, the pattern was more similar to that of control cells, with the exception of the glycolytic capacity, which was found higher than that of control cells. Regarding the glycolytic reserve, we observed the same increase in both cadmium-treated samples (Fig. 3B).

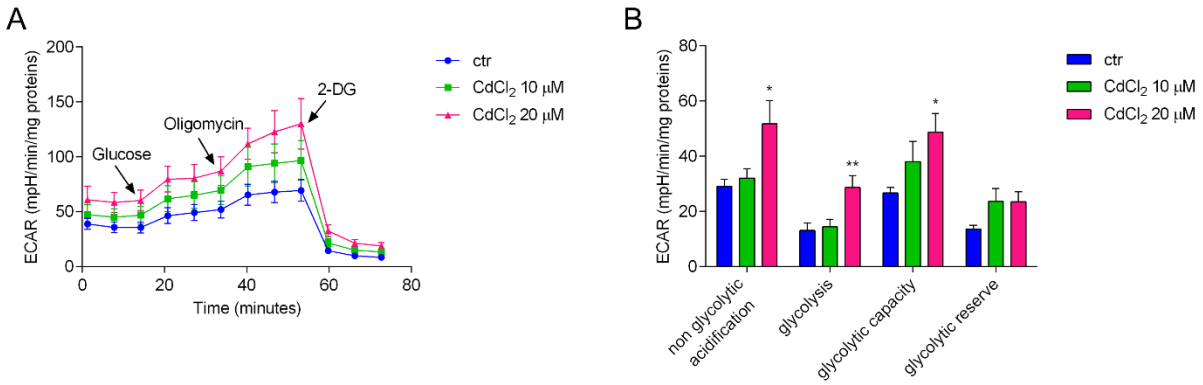

Fig. 3. Glycolytic functions analysis in cadmium treated cells. A) Representative ECAR profile of control and $CdCl_2$-treated cells of three independent experiments, expressed as mpH/min/mg proteins. The arrows indicate the time of addition of glucose, oligomycin and 2-DG. B) Analysis of different glycolytic parameters. Bars indicate the mean ± SEM obtained in three independent experiments.
Statistically significant: * $p < 0.05$, ** $p < 0.01$

The cells possess the ability to switch from glycolysis to oxidative phosphorylation in response to environmental changes for energy production; this adaptation can be investigated using the Glycolytic Rate Assay. We measured the basal glycolytic rate and the compensatory glycolysis following mitochondrial inhibition in SH-SY5Y cells previously treated with either 10 µM or 20 µM of $CdCl_2$ for 24 hours (Fig. 4). The proton efflux rate (PER) is sustained by both mitochondrial respiration and glycolysis in all conditions. The injection of rotenone and antimycin A, responsible for mitochondrial complex I and complex III inhibition, triggered a higher compensatory glycolysis in cadmium-treated cells, probably due to higher glycolytic capacity and reserve. When 2-DG was added, the PER was minimized, but the rate of acidification measured was still higher in treated cells compared to control cells (Fig. 4A).

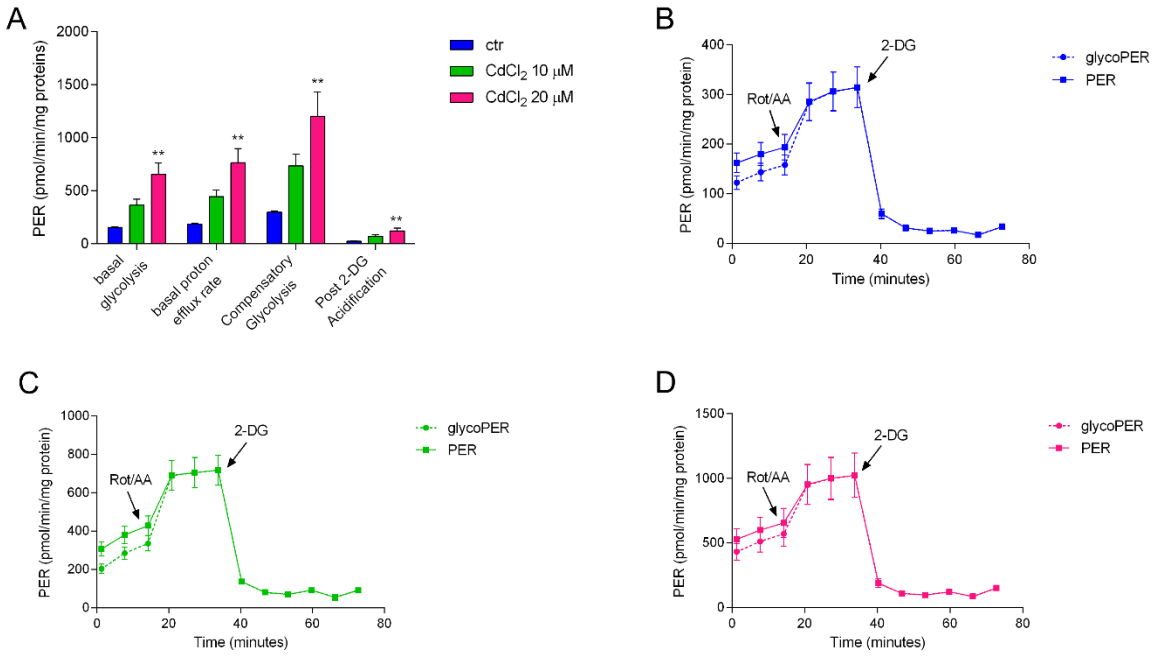

Fig. 4. Evaluation of basal and compensatory glycolysis after cadmium treatment in neuronal cells. Analysis of basal and compensatory glycolytic levels in control and cadmium treated cells (A). Bars indicate the mean ± SEM obtained in three independent experiments. Representative PER and glycoPER profiles of control cells (B) and 10 µM $CdCl_2$ (C) or 20 µM $CdCl_2$ (D) treated cells of three independent experiments; results are expressed as pmol/min/mg proteins. The arrows indicate the time of rotenone/antimycin A and 2-DG addition.

Statistically significant: ** $p < 0.01$

3.4. $CdCl_2$ administration induces a higher ATP production rate through glycolysis

The increase in glycolytic rate, following $CdCl_2$ administration, suggested that cadmium could also act on total ATP production. The Seahorse ATP Rate Assay allows to calculate ATP production in living cells, distinguishing between the fraction of ATP produced by oxidative phosphorylation and the one produced by glycolysis.

$CdCl_2$ administration was found to increase the total ATP production rate (Fig. 5A). Moreover, cells treated with 10 µM $CdCl_2$ displayed a significantly higher glycolytic ATP level (Fig. 5E); on the other hand, cells treated with 20 µM $CdCl_2$ showed a decrease in ATP derived from oxidative phosphorylation, as well as an increase in glycolytic ATP (Fig. 5C and E).

Given the ATP production rate, it is also possible to calculate the relative contributions of glycolysis and oxidative phosphorylation to ATP production (Fig. 5B). Treatment with $CdCl_2$ caused a dose-dependent reduction in oxidative phosphorylation (Fig. 5D) and a specular dose-dependent increase in glycolysis, suggesting that most of the energy demand is supplied by glycolysis (Fig. 5F).

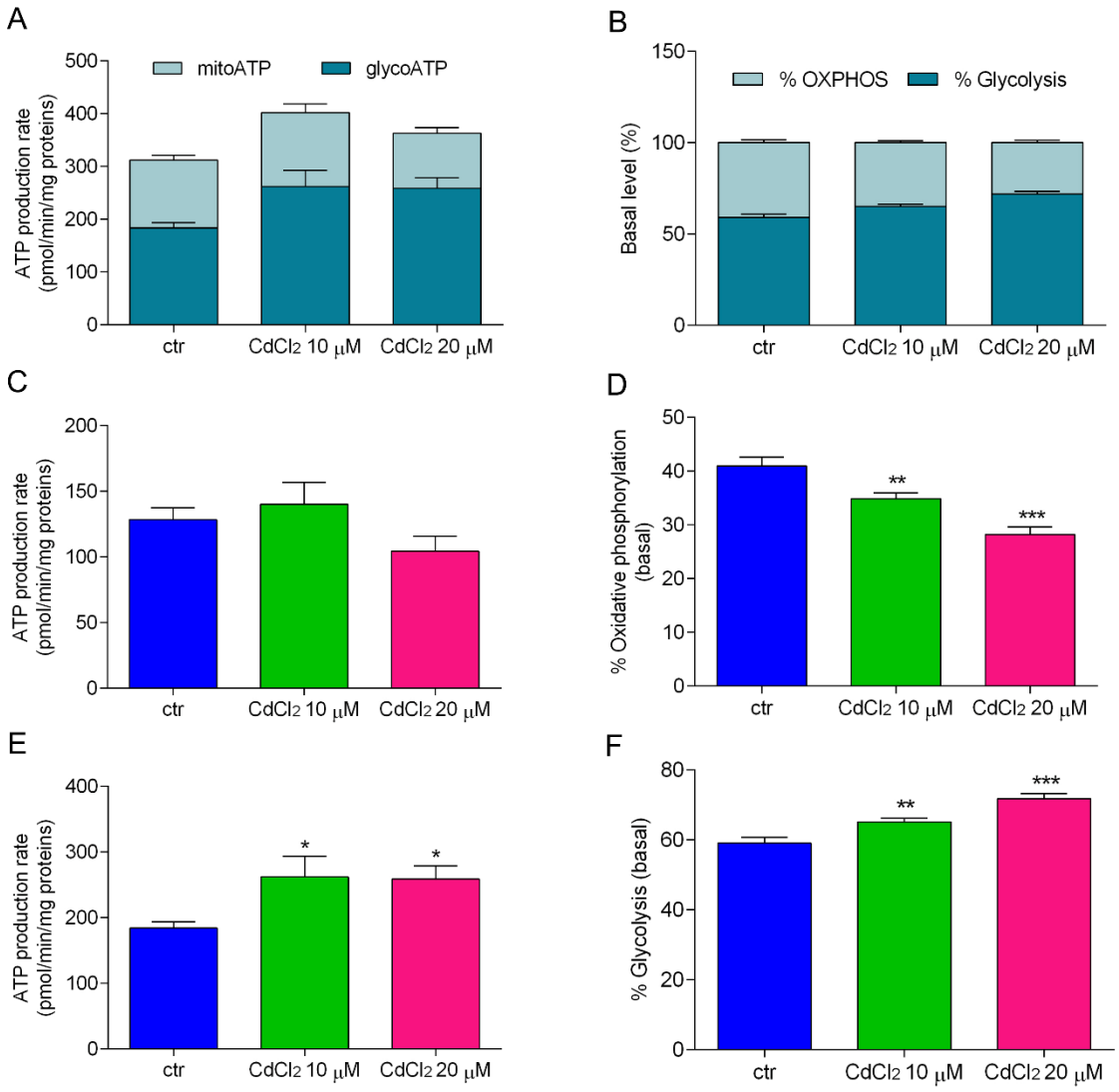

Fig. 5. ATP production in cadmium treated cells. Total (A), mitochondrial (C) and glycolytic (E) ATP production rate in neuronal cells treated for 24 hours with $CdCl_2$ (10 µM and 20 µM). Basal percentage level (B) of oxidative phosphorylation (D) and glycolysis (F). Bars indicate the mean ± SEM obtained in three independent experiments.

Statistically significant: * $p < 0.05$, ** $p < 0.01$, *** $p < 0.001$

3.5. $CdCl_2$ administration leads to a decrease in mitochondrial respiration

The investigation of ATP production after treatment with $CdCl_2$ showed a decrease in oxidative phosphorylation that led us to investigate mitochondrial functions through the Mito Stress Test.

As shown in Figure 6, the presence of 20 µM $CdCl_2$ reduced the oxygen consumption basal rate. The injection of the ATP synthase inhibitor oligomycin allowed to determine the mitochondrial ATP production rate, which was found significantly lower in 20 µM $CdCl_2$ treated cells (Fig. 6B). Following oligomycin addition, we also observed a decrease in OCR rate and an increase in ECAR level (Fig. 6A and C). Subsequently, OCR level increased after FCCP injection, allowing the evaluation of the maximal respiration rate, as well as the spare respiratory capacity. $CdCl_2$ administration caused a significant reduction in the maximal respiration rate at 20

µM $CdCl_2$, while the spare respiratory capacity significantly increased in treated cells at both $CdCl_2$ concentrations. Rotenone and antimycin A injection inhibited mitochondrial oxygen consumption leading to a sharp decrease in OCR level; however, the oxygen consumption not linked to mitochondria was found to be the same for all the conditions tested (Fig 6A and B). Finally, the coupling efficiency did not show any difference among the samples (Fig. 6D).

Taken together these results indicate a lower mitochondrial efficiency in respiration and energy production, following treatment with $CdCl_2$.

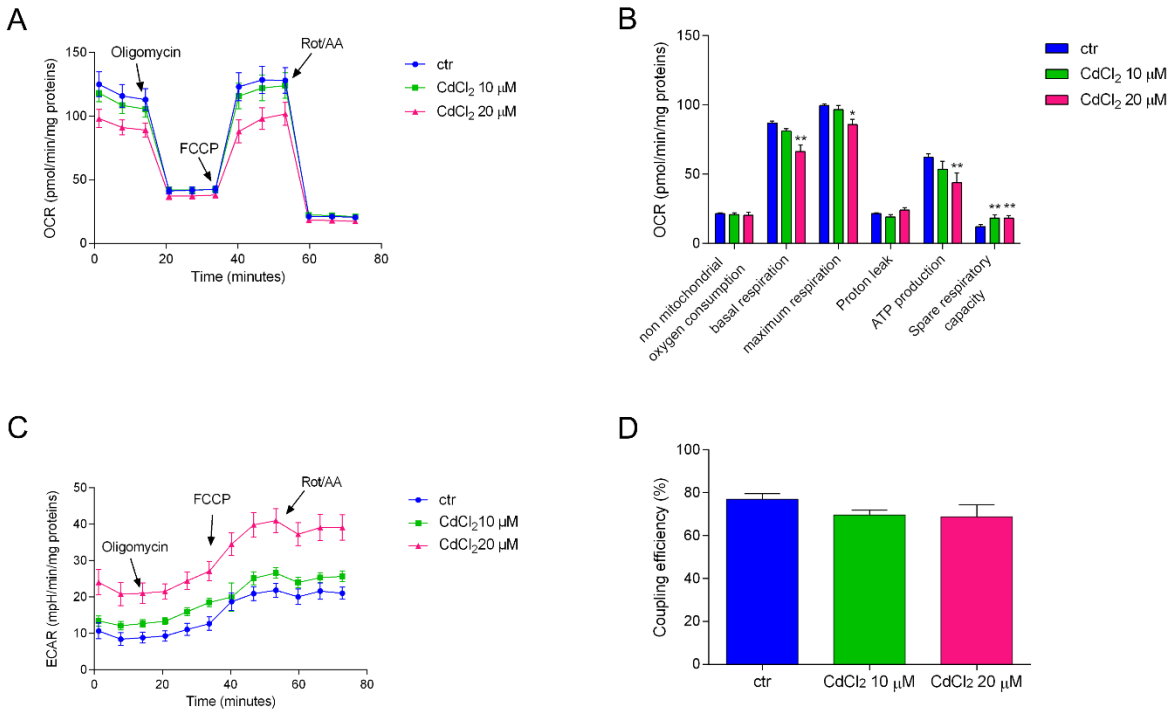

Fig. 6. Mitochondrial functionality in SH-SY5Y cells treated with 10 µM and 20 µM $CdCl_2$. OCR (A) and ECAR (C) traces, expressed as pmol O_2/min/mg proteins and mpH/min/mg proteins respectively, in control and cadmium treated cells. The arrows indicate the time of addition of oligomycin, FCCP and rotenone/antimycin A. Analysis of key mitochondrial parameters (B) and coupling efficiency (D). Bars indicate the mean ± SEM obtained in three independent experiments.

Statistically significant: * $p < 0.05$, ** $p < 0.01$

3.6. Mitochondrial fuel oxidation pattern changes when neuronal cells are treated with cadmium

The Mito Fuel Flex test is used to investigate fuels oxidation by mitochondria in order to maintain OCR basal level. We analysed the oxidation of glucose, long-chain fatty acids and glutamine after 24 hours treatment with $CdCl_2$ at the concentrations of 10 µM and 20 µM (Fig. 7).

Analysing the dependency, i.e. the cells' reliance on a particular fuel pathway to maintain baseline respiration, we saw that, for all the conditions studied, half of the total dependency was linked to glucose oxidation: in control cells, the other half dependency was nearly equally distributed between glutamine and fatty acids, while, following treatment with $CdCl_2$, glutamine dependency increased and fatty acids dependency decreased

(Fig. 7B, D, F). In fact, Figure 8C and E show that the fatty acids dependency decreased in a dose-dependent way, while glutamine dependency was significantly higher in cadmium treated cells.

The evaluation of fuel capacity, i.e. the ability possessed by mitochondria to oxidize a fuel when other fuel pathways are inhibited, allows to calculate the fuel flexibility, which is the ability of the cells to increase oxidation of a particular fuel in order to compensate the inhibition of alternative fuel pathways. The fuel capacity linked to glucose oxidation was reduced at increasing $CdCl_2$ doses, leading to a significant reduction in fuel flexibility (Fig. 7A). Instead, the fuel flexibility of fatty acids remained constant due to the cadmium induced decrease in both dependency and capacity (Fig. 7C). Interestingly, glutamine flexibility was completely abolished in $CdCl_2$-treated cells, due to the increase in dependency and the lack of variation in capacity (Fig. 7E).

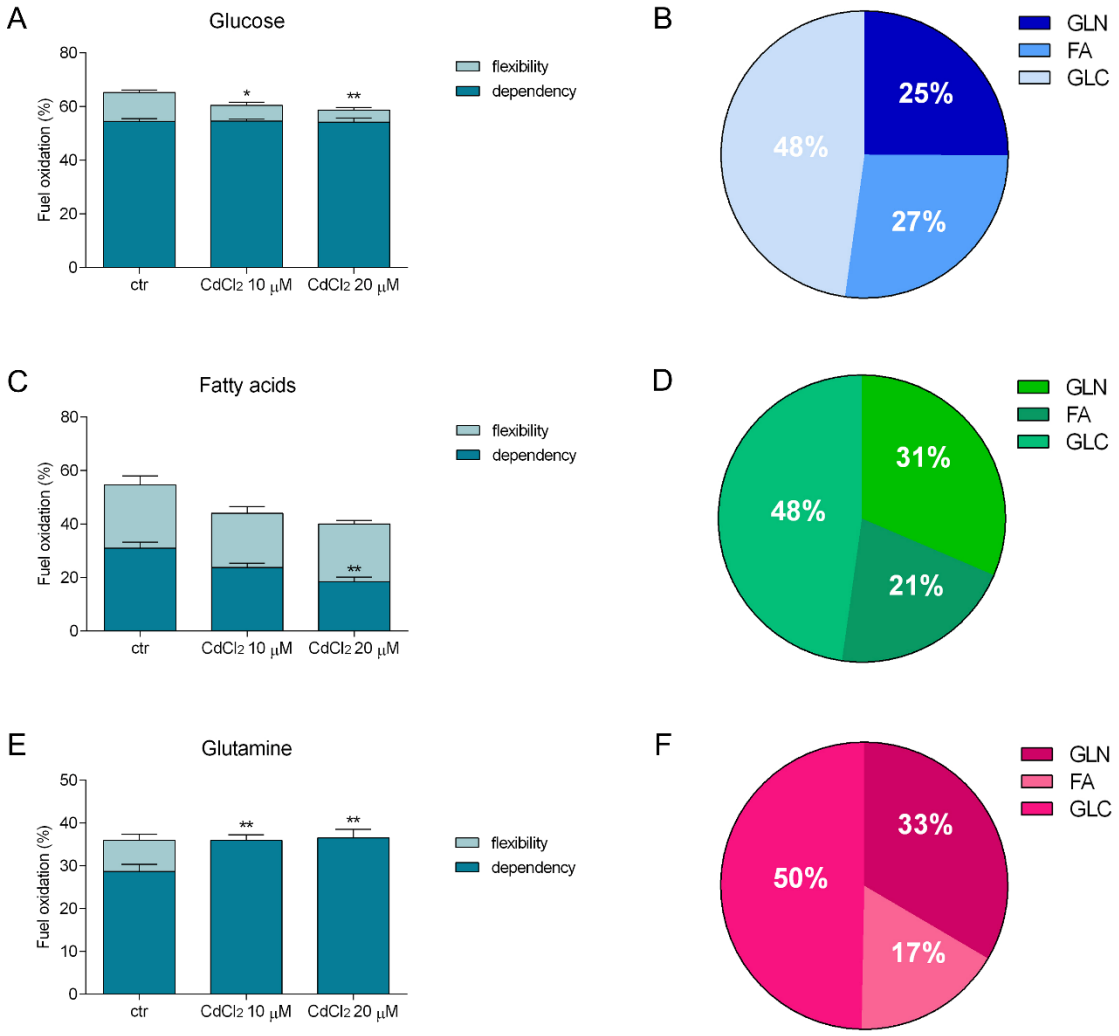

Fig. 7. Evaluation of mitochondrial fuel oxidation in SH-SY5Y Cd-treated cells. Glucose (A), long-chain fatty acids (C) and glutamine (E) mitochondrial fuel oxidation dependency and flexibility. Bars indicate the mean ± SEM obtained in three independent experiments. Pie charts of control cells (B), 10 µM $CdCl_2$ (D) and 20 µM $CdCl_2$ (F) fuel dependency.

Statistically significant: * $p < 0.05$, ** $p < 0.01$

3.7. Cadmium exposure increases oxidative stress

One of the main mechanisms of cadmium toxicity is increasing oxidative stress, leading in turn to lipid peroxidation and to a decrease in antioxidant defences. In order to understand SH-SY5Y oxidative status, after 24 hours exposure to either 10 µM or 20 µM $CdCl_2$, lipid peroxidation and glutathione levels, as well as the activity of glutathione reductase (GR) and glutathione S-transferase (GST) were analysed.

Our data showed an increase in lipid peroxidation levels in cadmium treated cells, slightly higher at 10 µM $CdCl_2$ than at 20 µM $CdCl_2$ (Fig. 8A), as well as a significant increase in the total glutathione level (Fig. 8B). Moreover, we observed a nearly 2-fold increase in oxidized glutathione (GSSG) level, with a consequent decrease in the reduced, scavenging form (GSH), after incubation with $CdCl_2$ (Fig. 8C).

Enzyme assays performed on two enzymes involved in the glutathione metabolism, GST and GR, did not show any statistically significant variation (Fig. 8D).

Taken together these results showed an increase in oxidative stress level in cadmium treated cells, that could possibly affect energy metabolism.

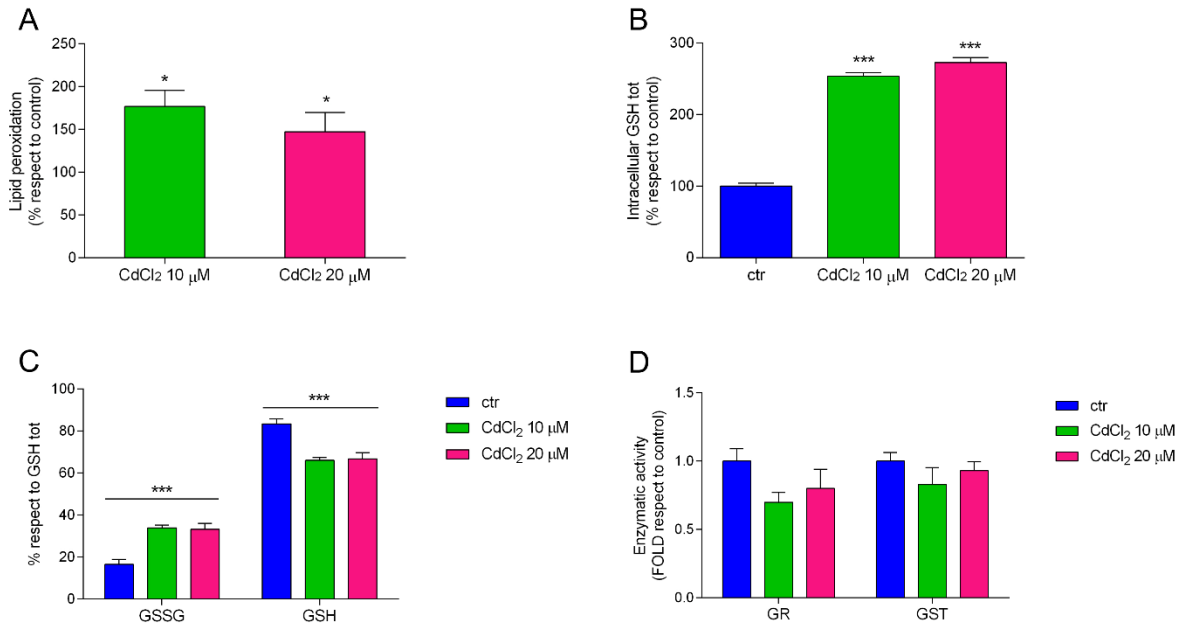

Fig. 8. Oxidative stress status after 10 µM and 20 µM $CdCl_2$ 24-hour administration. A) Lipid peroxidation level expressed as a percentage of the control. B-C) Total glutathione level (B) and GSSG and GSH (C) levels, expressed as percentages of total glutathione in cadmium treated and untreated cells. D) Glutathione reductase (GR) and glutathione S-transferase (GST) activities, expressed as folds respect to control. Data are shown as means ± standard error (SEM).

Statistically significant: *$p<0.05$, ***$p<0.001$

4. Discussion

The metabolic analysis, performed through Seahorse, allowed to gain some insights into the metabolic rearrangements induced by cadmium, a toxic and widely diffused metal and a recognized carcinogen. Cadmium toxicity is mainly due to an increase in oxidative stress, as well as to its ability to substitute zinc in hundreds of zinc-proteins (Satarug et al., 2018; Urani et al., 2015). Cadmium has been also associated to neurodegenerative diseases pathogenesis: oxidative stress has been demonstrated to play an essential role in ALS, as well as in Parkinson and Alzheimer disease, pathogenesis (Singh et al., 2019; Sultana et al., 2013). These data, along with our previous results (Forcella et al., 2020), prompted us to deeply investigate the effect of sublethal $CdCl_2$ concentrations on human neuroblastoma SH-SY5Y cultured cells, as possible mechanisms of induced neurodegeneration.

Seahorse analysis showed an increase in glycolytic basal level following cadmium administration, as shown by Glycolysis Stress Test and Glycolytic Rate Assay: this increase was found significant in the presence of 20 µM $CdCl_2$, although an increasing trend was already evident following 10 µM $CdCl_2$ administration. However, Cell Energy Phenotype analysis showed that cadmium administration reduced the ability to supply energy demand via glycolysis in the presence of stressor compounds, like the simultaneous administration of oligomycin and FCCP. Glycolytic capacity, the cell's ability to use glycolysis to its maximum capacity, was also increased upon $CdCl_2$ administration, while the glycolytic reserve, indicating how close the glycolytic function is to the cell theoretical maximum, was also increased, but to the same extent at both $CdCl_2$ concentrations. This could be due to the fact that basal glycolysis increased to higher levels after 20 µM $CdCl_2$ administration and/or to the fact that the theoretical maximum has been reached. Glycolysis Stress Test also showed a higher basal acidification level for cadmium treated cells, measured in the absence of glucose, which can be due to cadmium promoting amino acids breakdown to yield acetylCoA to fuel Krebs cycle; in fact, mitochondrial fuel oxidation pattern analysis showed that cadmium treated cells rely strongly on glutamine to maintain baseline respiration. The ECAR measured in this case would therefore be partly due to CO_2, explaining why the acidification level remained high, following glycolysis inhibition by 2-DG, in cadmium treated cells.

The fact that oligomycin alone was able to induce an increase in the glycolytic capacity of cadmium treated cells suggests that these cells rely more on glycolysis than on oxidative phosphorylation for ATP production. This is confirmed by Seahorse ATP Rate assay showing that, following cadmium administration, ATP is increasingly produced by glycolysis, in a dose dependent way, while the relative contribution of oxidative phosphorylation to ATP production decreases. The analysis of PER and glycoPER showed that cadmium treated cells are endowed with a higher compensatory glycolysis, whose value becomes significant after administration of 20 µM $CdCl_2$, although an increase is evident also following 10 µM $CdCl_2$ administration. The ratio between PER and glycoPER confirms that the relative contribution of glycolysis to acidification increases with cadmium administration in a dose dependent way.

The switch to glycolysis for ATP production is also demonstrated by the Mito Stress Test, showing that cadmium administration leads to a decrease in basal respiration rate in a dose dependent way; this is mirrored

by the lower increase, in cadmium treated cells, in maximum respiration, following the uncoupler FCCP addition. As previously observed in healthy murine C3H cells (Oldani et al., 2020), cadmium led to an increase in the spare respiratory capacity, which, for SH-SY5Y cells is similar for both $CdCl_2$ concentration, suggesting that the cell theoretical maximum had been reached. Although cadmium administration did not alter mitochondrial coupling efficiency, these data show that it interfered with mitochondrial respiration, leading to a decrease in mitochondrial ATP production, which was found significant only after 20 μM $CdCl_2$ administration, but could be detected also after 10 μM $CdCl_2$ administration. The higher ability of cadmium treated cells to compensate with glycolysis after mitochondrial respiration inhibition can be correlated to their higher glycolytic capacity and reserve.

The increase in glycolysis promoted by cadmium administration to SH-SY5Y cells is well in accordance with our previously reported data on C3H healthy fibroblast treated with cadmium (Oldani et al., 2020). This is likely at the basis of the malignant cell transformation induced by cadmium, a well-known carcinogen: however, our data show that cadmium is able to hyperactivate glycolysis also in cancer cells like SH-SY5Y cells. These cells already rely on glycolysis more than oxidative phosphorylation for ATP production, with more than 50% ATP produced by glycolysis, a much higher value compared with the 12% normally measured in healthy cells (Seyfried and Shelton, 2010); our measurements also show that basal glycolysis, measured as glycoPER, is much higher in SH-SY5Y cells (over 100 pmol/min/mgprotein) than in C3H cells (50 pmol/min/mgprotein), reflecting their cancer nature.

Besides increasing glutamine dependency of SH-SY5Y cells, cadmium administration induced other rearrangements in mitochondrial fuel oxidation pattern. Both control and cadmium-treated cells were found equally dependent on glucose as a fuel, reflecting the fact that they are all cancer cells; however, cadmium decreased cell capacity to use glucose as a fuel when both lipid and glutamine utilization pathways were blocked: as a consequence, fuel flexibility was also decreased. Lipid dependency was decreased by cadmium administration in a dose dependent way, as well as the cell capacity to use lipids as a fuel when other fuels pathways cannot be used; as a result of a decrease in both lipid dependency and capacity, flexibility remained constant. Finally, the increase in glutamine dependency, mentioned above, was not accompanied by any variation in glutamine capacity, showing that the cells cannot increase their ability to use glutamine as a fuel when other fuels pathways are blocked; as a result cadmium administration abolished flexibility. The increase in glutamine dependency was found similar at both $CdCl_2$ concentrations, suggesting that a maximum has been reached in glutamine supply. Moreover, this explains the decrease in lipid dependency, since glutamine enters Krebs cycle as α-ketoglutarate to yield citrate; the latter can be translocated into the cytosol where it is converted by citrate lyase into oxalacetate and acetylCoA, which is carboxylated to malonylCoA, producing fatty acids.

Increased glutamine consumption also involves increased glutamate production, which could be used for glutathione synthesis, together with glycine and cysteine produced from glycolytic intermediates; this could be a defensive mechanism against oxidative stress triggered by cadmium and could explain the increase in total glutathione observed in our experiments. However, the GSSG/GSH ratio is increased following cadmium

administration and, although cell death is prevented, lipid peroxidation could be detected in cells treated with cadmium. Other cell defense mechanisms against oxidative stress play an important role, like metallothioneines, whose expression is induced in SH-SY5Y cells following cadmium treatment (Forcella et al., 2020); however, GSH is essential for neuronal cells and is normally supplied also by microglia. Further work will address the role of GSH in the protection against cadmium toxicity in neuronal cells.

5. Conclusions

Overall, cadmium exposure caused alterations in the oxidative balance of human neuronal cells, that led to a rearrangement of the energy metabolism, with an increase in glycolysis and in glutamine dependency. This is probably linked to the observed higher total glutathione level, since glutamine can lead to a higher glutamate production, that could be used for glutathione synthesis, together with glycine and cysteine produced by glycolytic intermediates.

Author contributions

Federica Bovio: Data curation, Formal analysis, Investigation, Validation, Visualization, Writing - review & editing; **Pasquale Melchioretto:** Investigation; **Matilde Forcella:** Conceptualization, Methodology, Project administration, Supervision, Writing - original draft, Writing - review & editing; **Paola Fusi:** Conceptualization, Funding acquisition, Methodology, Project administration, Resources, Writing - original draft, Writing - review & editing; **Chiara Urani:** Funding acquisition, Project administration, Resources, Writing - review & editing.

Funding

This work was supported by the University of Milano-Bicocca (2019-ATE-0373 to PF) and partially supported by the Italian Ministry (2017-NAZ-0387 to CU).

Conflict of interest statement

The authors declare no conflict of interest.

References

Al-Ghafari, A., Elmorsy, E., Fikry, E., Alrowaili, M., Carter, W.G., 2019. The heavy metals lead and cadmium are cytotoxic to human bone osteoblasts via induction of redox stress. PLoS One 14, e0225341. https://doi.org/10.1371/journal.pone.0225341

Bradford, M.M., 1976. A rapid and sensitive method for the quantitation of microgram quantities of protein utilizing the principle of protein-dye binding. Anal. Biochem. 72, 248–254. https://doi.org/10.1006/abio.1976.9999

Branca, J.J.V., Fiorillo, C., Carrino, D., Paternostro, F., Taddei, N., Gulisano, M., Pacini, A., Becatti, M.,

2020. Cadmium-induced oxidative stress: Focus on the central nervous system. Antioxidants 9, 1–21. https://doi.org/10.3390/antiox9060492

Brand, M.D., 2016. Mitochondrial generation of superoxide and hydrogen peroxide as the source of mitochondrial redox signaling. Free Radic. Biol. Med. 100, 14–31. https://doi.org/10.1016/j.freeradbiomed.2016.04.001

Buege, J.A., Aust, S.D., 1978. Microsomal lipid peroxidation. Methods Enzymol. 52, 302–310. https://doi.org/10.1016/s0076-6879(78)52032-6

Cannino, G., Ferruggia, E., Luparello, C., Rinaldi, A.M., 2009. Cadmium and mitochondria. Mitochondrion 9, 377–384. https://doi.org/10.1016/j.mito.2009.08.009

Cuypers, A., Plusquin, M., Remans, T., Jozefczak, M., Keunen, E., Gielen, H., Opdenakker, K., Nair, A.R., Munters, E., Artois, T.J., Nawrot, T., Vangronsveld, J., Smeets, K., 2010. Cadmium stress: an oxidative challenge. Biometals an Int. J. role Met. ions Biol. Biochem. Med. 23, 927–940. https://doi.org/10.1007/s10534-010-9329-x

Forcella, M., Lau, P., Oldani, M., Melchioretto, P., Bogni, A., Gribaldo, L., Fusi, P., Urani, C., 2020. Neuronal specific and non-specific responses to cadmium possibly involved in neurodegeneration: A toxicogenomics study in a human neuronal cell model. Neurotoxicology 76, 162–173. https://doi.org/https://doi.org/10.1016/j.neuro.2019.11.002

Genchi, G., Sinicropi, M.S., Lauria, G., Carocci, A., Catalano, A., 2020. The Effects of Cadmium Toxicity. Int. J. Environ. Res. Public Health 17. https://doi.org/10.3390/ijerph17113782

Habig, W.H., Pabst, M.J., Jakoby, W.B., 1974. Glutathione S-transferases. The first enzymatic step in mercapturic acid formation. J. Biol. Chem. 249, 7130–7139.

Li, L., Tian, X., Yu, X., Dong, S., 2016. Effects of Acute and Chronic Heavy Metal (Cu, Cd, and Zn) Exposure on Sea Cucumbers (*Apostichopus japonicus*). Biomed Res. Int. 2016, 4532697. https://doi.org/10.1155/2016/4532697

Mezynska, M., Brzóska, M.M., 2018. Environmental exposure to cadmium—a risk for health of the general population in industrialized countries and preventive strategies. Environ. Sci. Pollut. Res. 25, 3211–3232. https://doi.org/10.1007/s11356-017-0827-z

Nordberg, G.F., 2009. Historical perspectives on cadmium toxicology. Toxicol. Appl. Pharmacol. 238, 192–200. https://doi.org/10.1016/j.taap.2009.03.015

Oh, S.-H., Lim, S.-C., 2006. A rapid and transient ROS generation by cadmium triggers apoptosis via caspase-dependent pathway in HepG2 cells and this is inhibited through N-acetylcysteine-mediated catalase upregulation. Toxicol. Appl. Pharmacol. 212, 212–223. https://doi.org/10.1016/j.taap.2005.07.018

Oldani, M., Manzoni, M., Villa, A.M., Stefanini, F.M., Melchioretto, P., Monti, E., Forcella, M., Urani, C., Fusi, P., 2020. Cadmium elicits alterations in mitochondrial morphology and functionality in C3H10T1/2Cl8 mouse embryonic fibroblasts. Biochim. Biophys. Acta - Gen. Subj. 1864, 129568. https://doi.org/https://doi.org/10.1016/j.bbagen.2020.129568

Peña-Bautista, C., Vento, M., Baquero, M., Cháfer-Pericás, C., 2019. Lipid peroxidation in neurodegeneration. Clin. Chim. Acta 497, 178–188. https://doi.org/10.1016/j.cca.2019.07.037

Sabir, S., Akash, M.S.H., Fiayyaz, F., Saleem, U., Mehmood, M.H., Rehman, K., 2019. Role of cadmium and arsenic as endocrine disruptors in the metabolism of carbohydrates: Inserting the association into perspectives. Biomed. Pharmacother. 114, 108802. https://doi.org/10.1016/j.biopha.2019.108802

Sabolić, I., Breljak, D., Škarica, M., Herak-Kramberger, C.M., 2010. Role of metallothionein in cadmium traffic and toxicity in kidneys and other mammalian organs. BioMetals 23, 897–926. https://doi.org/10.1007/s10534-010-9351-z

Sarkar, A., Ravindran, G., Krishnamurthy, V., 2013. a Brief Review on the Effect of Cadmium Toxicity: From Cellular To Organ Level. Int. J. Bio-Technology Res. 3, 2249–6858.

Satarug, S., Nishijo, M., Ujjin, P., Moore, M.R., 2018. Chronic exposure to low-level cadmium induced zinc-copper dysregulation. J. trace Elem. Med. Biol. organ Soc. Miner. Trace Elem. 46, 32–38. https://doi.org/10.1016/j.jtemb.2017.11.008

Seyfried, T.N., Shelton, L.M., 2010. Cancer as a metabolic disease. Nutr. Metab. (Lond). 7, 7. https://doi.org/10.1186/1743-7075-7-7

Singh, A., Kukreti, R., Saso, L., Kukreti, S., 2019. Oxidative Stress: A Key Modulator in Neurodegenerative Diseases. Molecules 24. https://doi.org/10.3390/molecules24081583

Sultana, R., Perluigi, M., Butterfield, D.A., 2013. Lipid peroxidation triggers neurodegeneration: A redox proteomics view into the Alzheimer disease brain. Free Radic. Biol. Med. 62, 157–169. https://doi.org/10.1016/j.freeradbiomed.2012.09.027

Thévenod, F., Fels, J., Lee, W.K., Zarbock, R., 2019. Channels, transporters and receptors for cadmium and cadmium complexes in eukaryotic cells: myths and facts. BioMetals 32, 469–489. https://doi.org/10.1007/s10534-019-00176-6

Tjälve, H., Henriksson, J., 1999. Uptake of metals in the brain via olfactory pathways. Neurotoxicology 20, 181–195.

Urani, C., Melchioretto, P., Bruschi, M., Fabbri, M., Sacco, M.G., Gribaldo, L., 2015. Impact of Cadmium on Intracellular Zinc Levels in HepG2 Cells: Quantitative Evaluations and Molecular Effects. Biomed Res Int 2015, 949514. https://doi.org/10.1155/2015/949514

Wang, B., Du, Y., 2013. Cadmium and its neurotoxic effects. Oxid. Med. Cell. Longev. 2013. https://doi.org/10.1155/2013/898034

Wang, Y., Oberley, L.W., Murhammer, D.W., 2001. Antioxidant defense systems of two lipidopteran insect cell lines. Free Radic. Biol. Med. 30, 1254–1262. https://doi.org/10.1016/s0891-5849(01)00520-2

Yang, Y., Estrada, E.Y., Thompson, J.F., Liu, W., Rosenberg, G.A., 2007. Matrix metalloproteinase-mediated disruption of tight junction proteins in cerebral vessels is reversed by synthetic matrix metalloproteinase inhibitor in focal ischemia in rat. J. Cereb. blood flow Metab. Off. J. Int. Soc. Cereb. Blood Flow Metab. 27, 697–709. https://doi.org/10.1038/sj.jcbfm.9600375

Zhang, H., Reynolds, M., 2019. Cadmium exposure in living organisms: A short review. Sci. Total Environ.

678, 761–767. https://doi.org/10.1016/j.scitotenv.2019.04.395

Zheng, W., Perry, D.F., Nelson, D.L., Aposhian, H.V., 1991. Choroid plexus protects cerebrospinal fluid against toxic metals. FASEB J. 5, 2188–2193. https://doi.org/10.1096/fasebj.5.8.1850706

Zong, L., Xing, J., Liu, S., Liu, Z., Song, F., 2018. Cell metabolomics reveals the neurotoxicity mechanism of cadmium in PC12 cells. Ecotoxicol. Environ. Saf. 147, 26–33. https://doi.org/10.1016/j.ecoenv.2017.08.028

Figure 1

Click here to access/download;Figure;Fig 1.tif

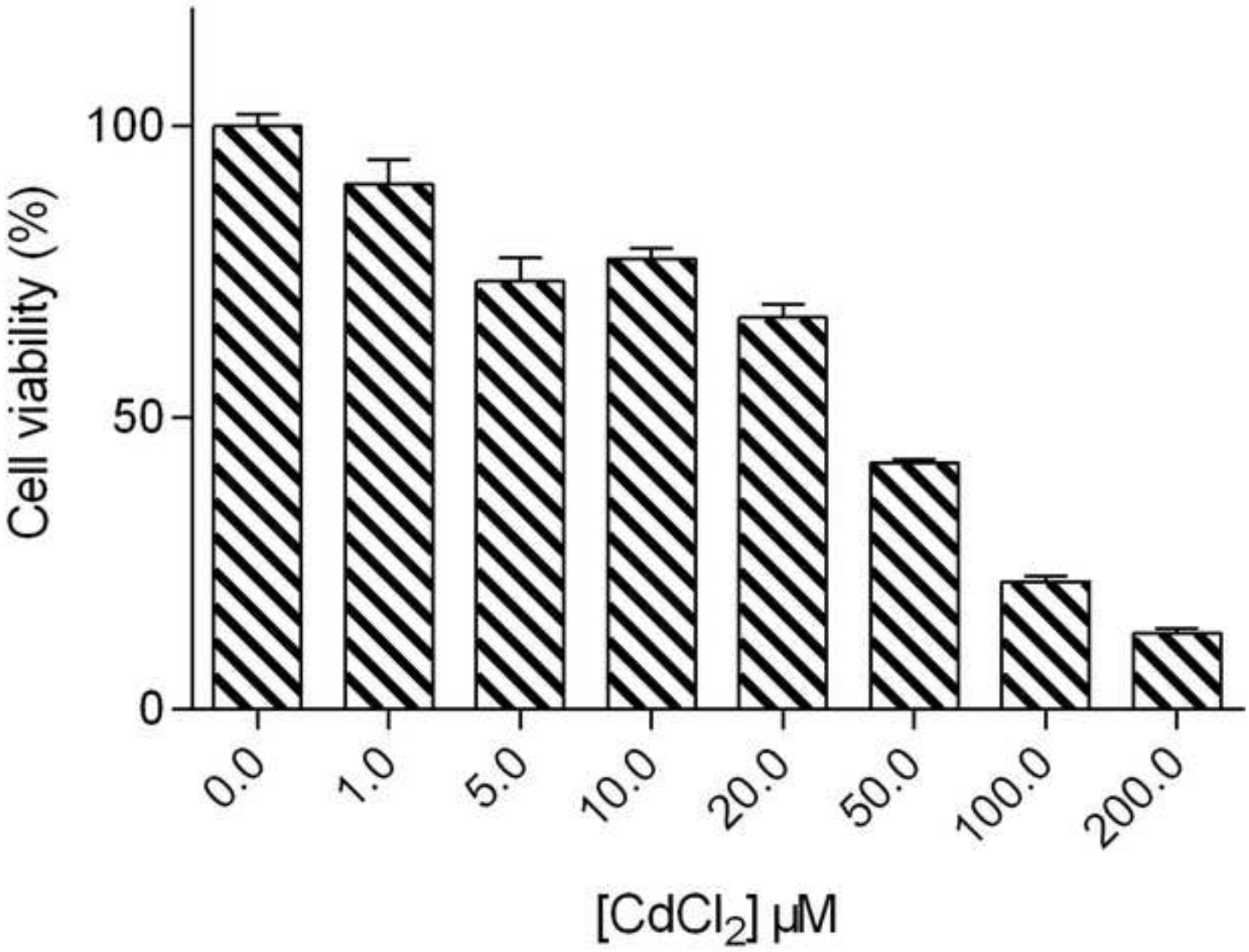

Figure 2

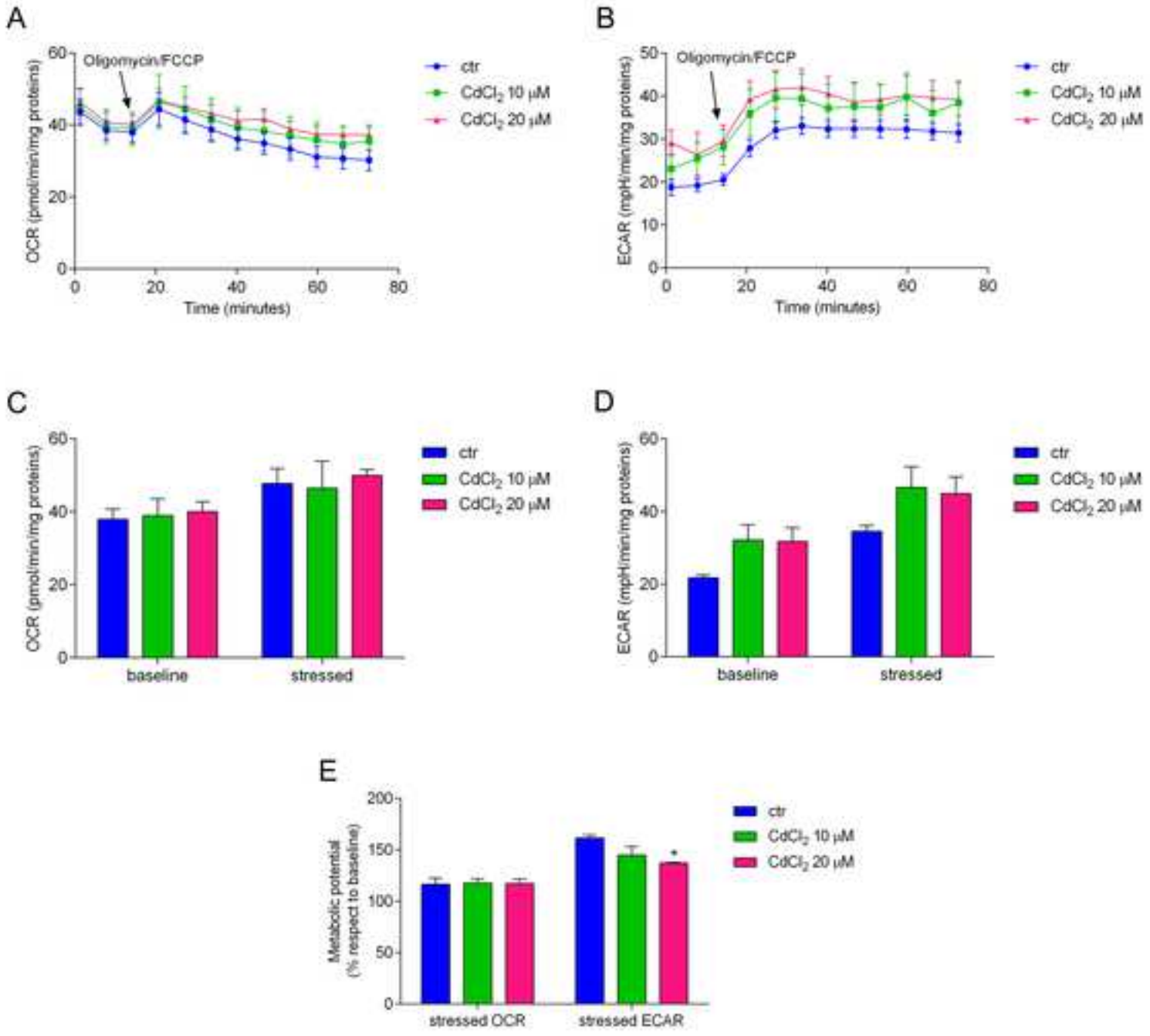

Figure 3

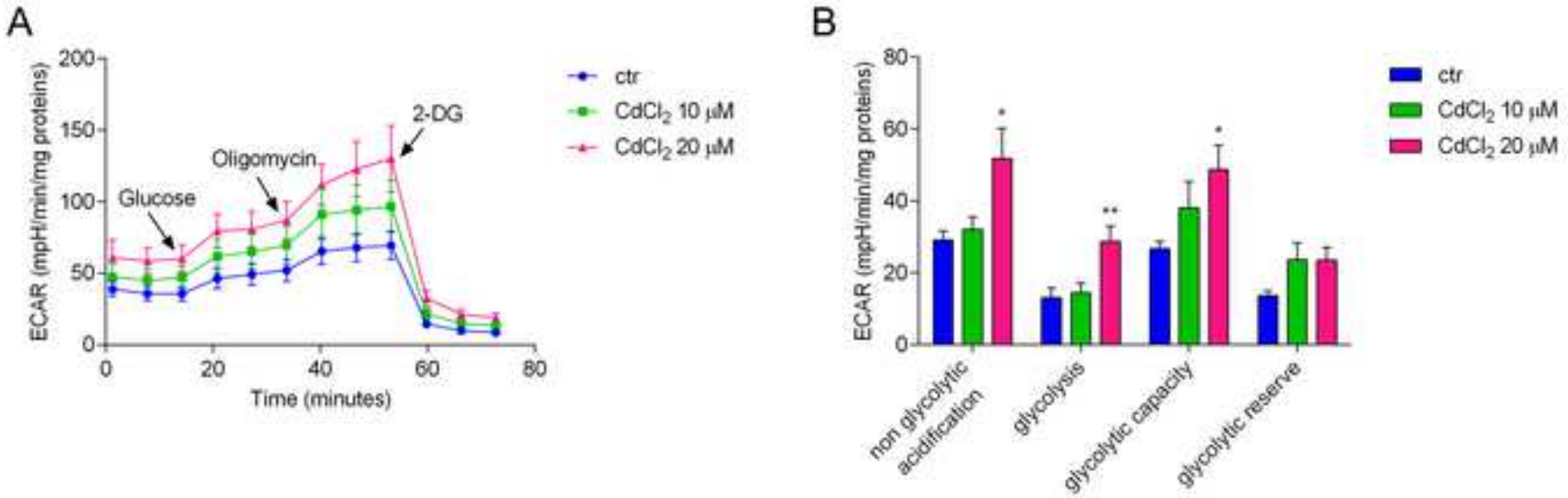

Figure 4

Click here to access/download;Figure;Fig 4.tif

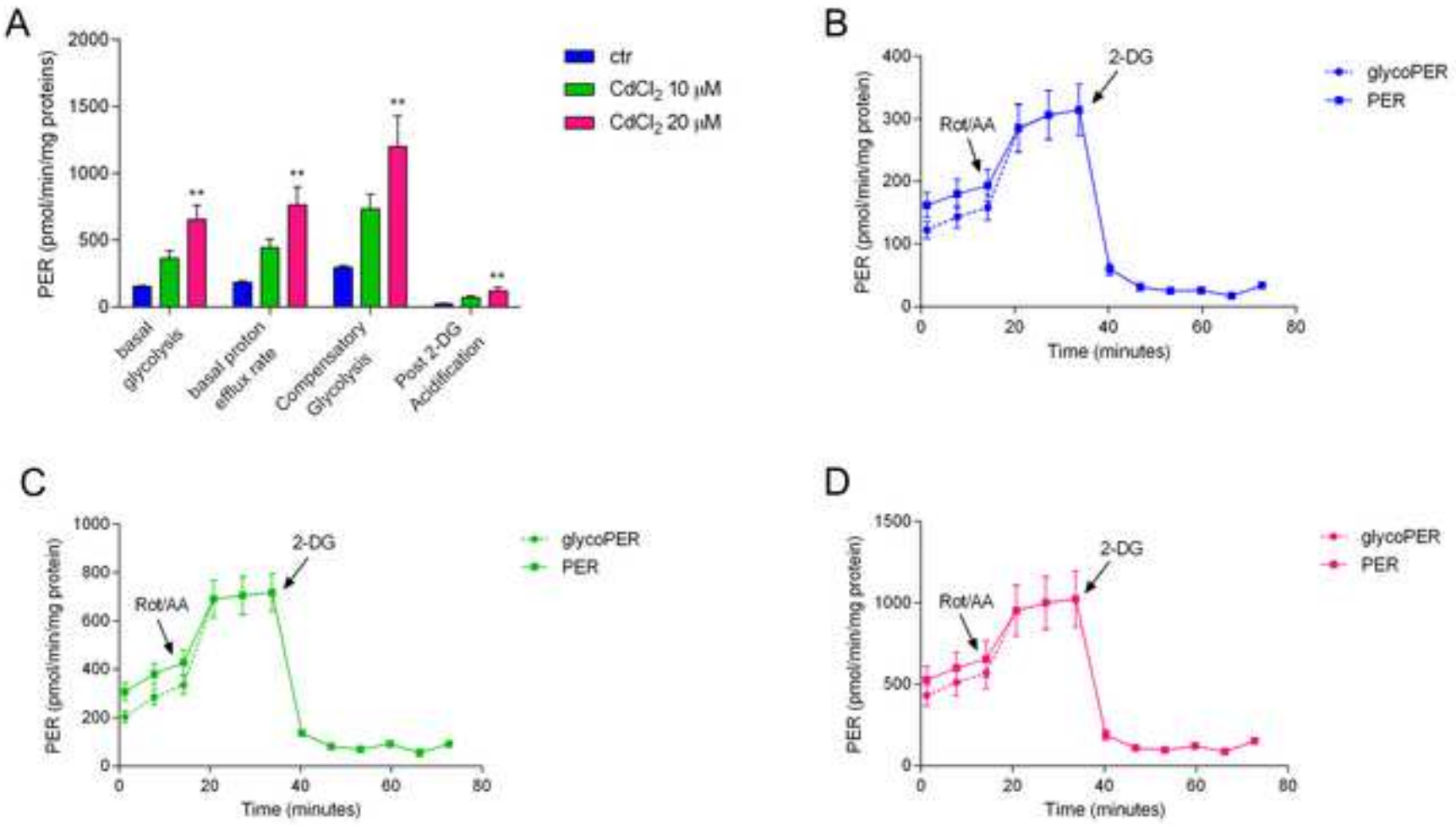

Figure 5

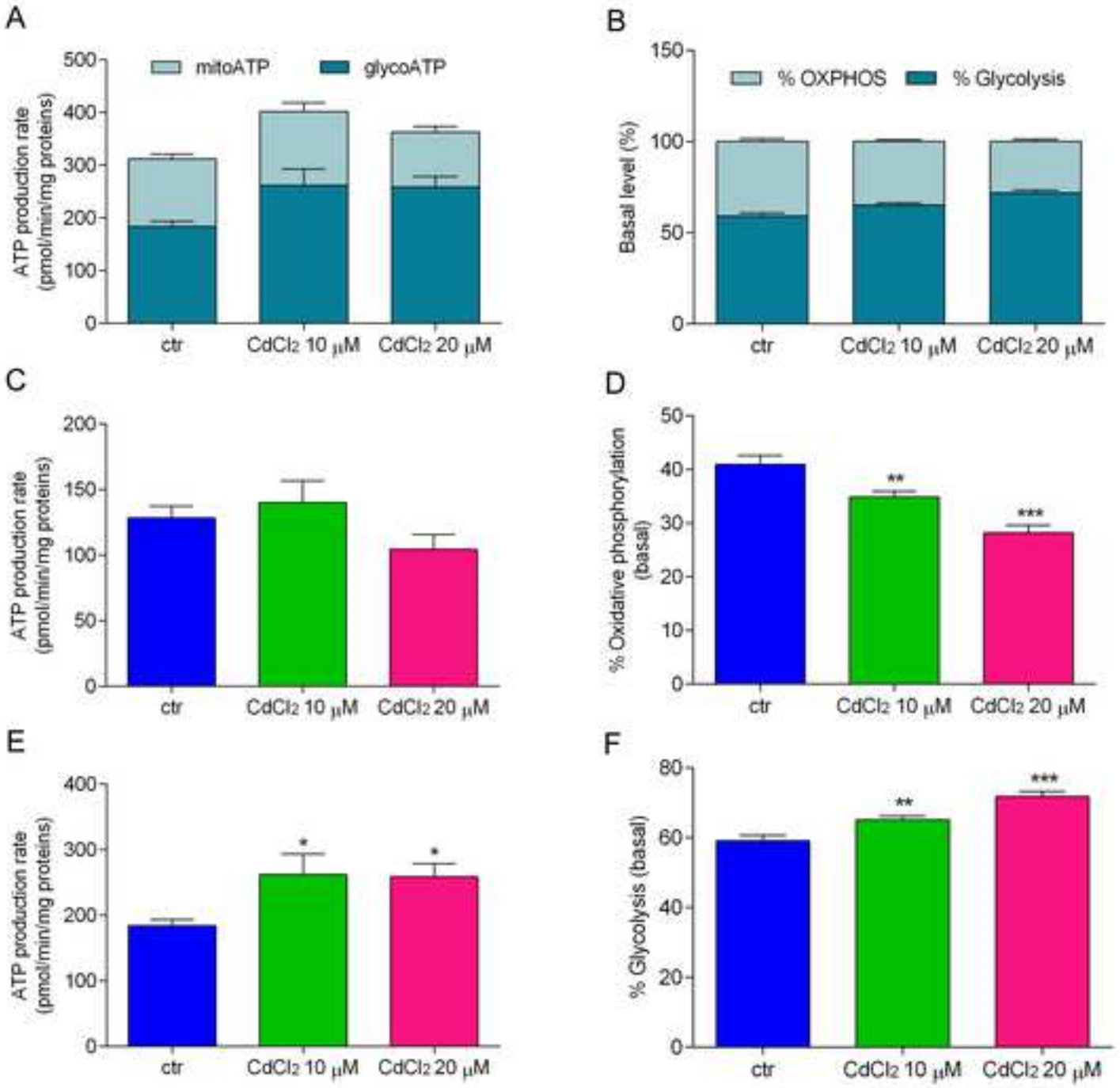

Figure 6

Click here to access/download;Figure;Fig 6.tif

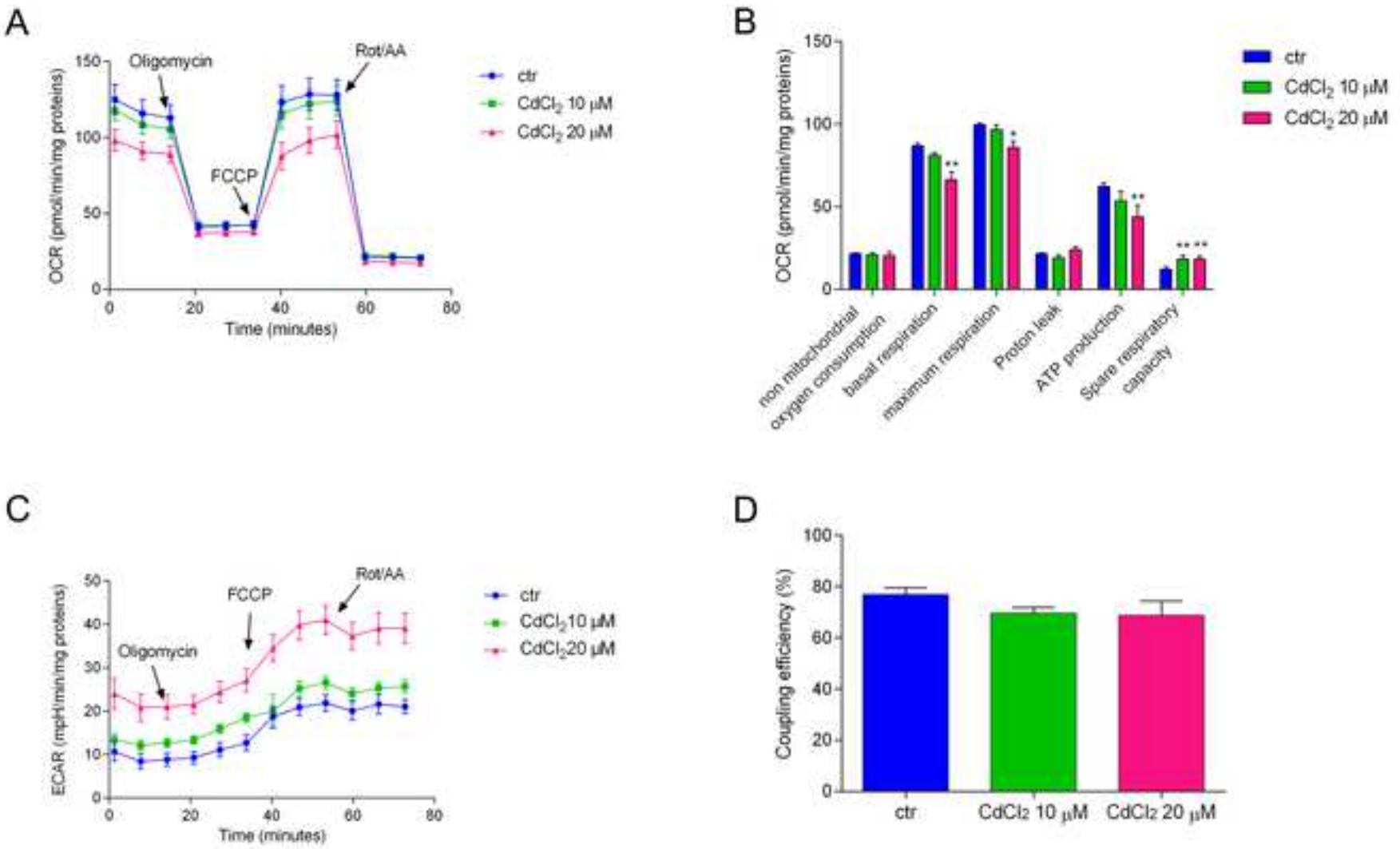

Figure 7

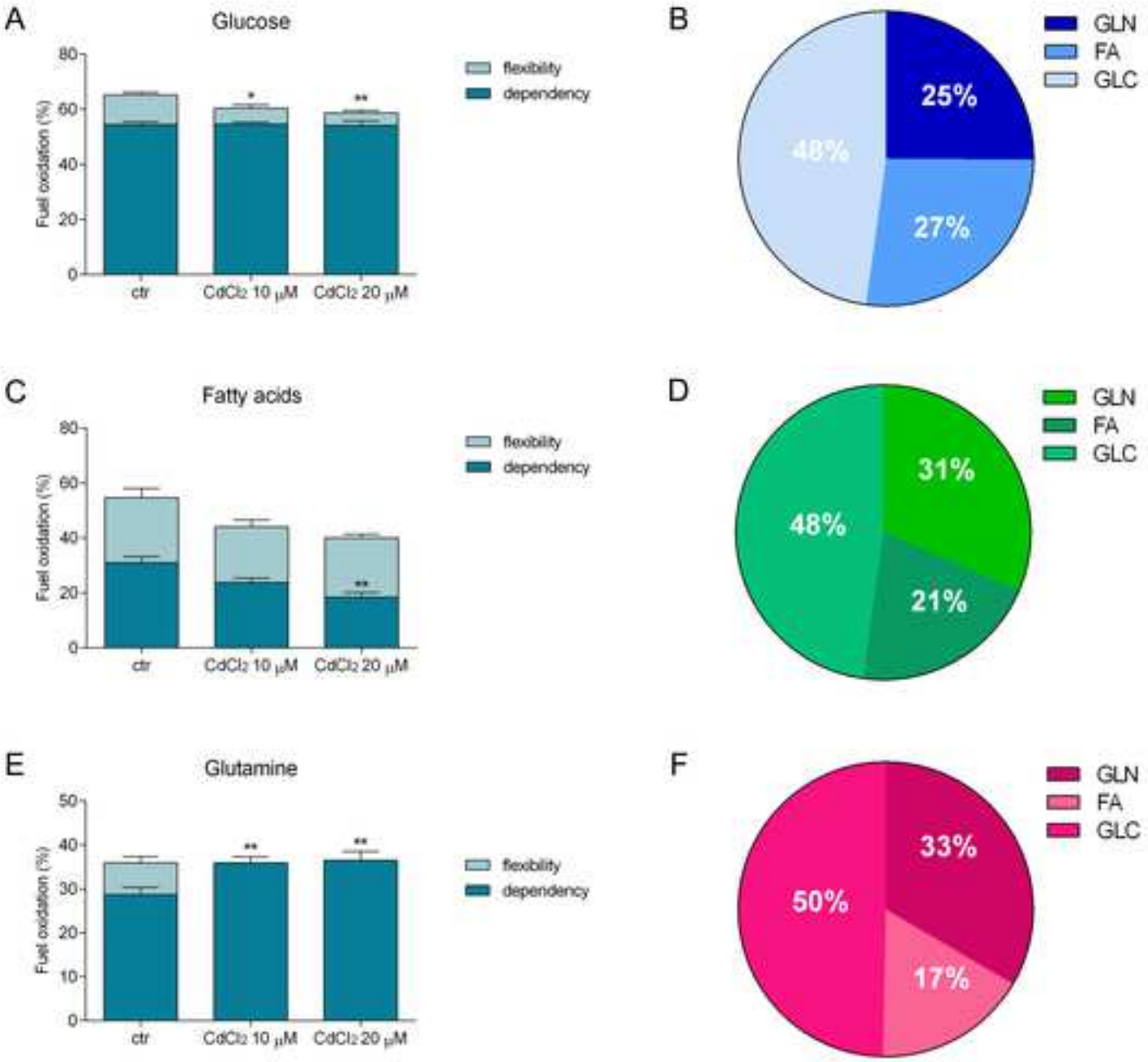

Figure 8

Click here to access/download;Figure;Fig 8.tif